Aerial Hyperspectral Analysis: Distinguishing Olive Varieties for Precision Agriculture

Ruth M. Córdoba Ortega, Alba Gómez Liébana
Researcher at the University of Jaén, Paraje Las Lagunillas Jaén, Spain
e-mail: rcortega@ujaen.es | aglieban@ujaen.es
M.Isabel Ramos
Dept. Cartographic, Geodetic and Photogrammetric Engineering.
University of Jaen
Jaen, Spain
e-mail: miramos@ujaen.es
Lidia M. Ortega, Juan M. Jurado
Researcher at the University of Jaén, Paraje Las Lagunillas Jaén, Spain
e-mail: lidia@ujaen.es | jjurado@ujaen.es

***Abstract*—Distinguishing olive varieties is essential for optimizing orchard management and oil quality. Hyper-Spectral Imaging (HSI) captures subtle spectral differences in leaf reflectance, surpassing conventional sensors. This study explores the use of drone-acquired HSI to differentiate Arbequina and Picual olives, two predominant varieties. The high spectral resolution of HSI enables precise varietal mapping, supporting more efficient and sustainable agriculture.**

***Keywords-Hyperspectral*; *olive*; *drone*; *agriculture*.**

I. Introduction

The identification of olive varieties is essential for optimizing orchard management, irrigation strategies, and oil quality control. Traditionally, this process has relied on expert knowledge, morphological analysis, or genetic testing, which are time-consuming, costly, and impractical for large-scale plantations. A more efficient alternative is Hyper-Spectral Imaging (HSI), which captures the spectral reflectance of plants across a wide range of wavelengths, allowing for precise differentiation between varieties.

HSI has proven to be highly effective in agricultural applications due to its ability to detect subtle biochemical and structural differences in plant tissues. Unlike multispectral imaging, which captures only a limited number of spectral bands, hyperspectral sensors provide continuous spectral information, enabling a more detailed analysis of plant characteristics. In the case of olive cultivation, this technology offers a non-invasive method for distinguishing between varieties based on their unique spectral signatures.

In this study, we investigate the potential of Unmanned Aerial Vehicle (UAV)-mounted hyperspectral sensors to classify olive varieties in a high-throughput manner. We focus on Arbequina and Picual, two of the most widely cultivated varieties in southern Spain, which exhibit distinct agronomic and oil composition traits. By analyzing spectral differences in leaf reflectance, we aim to demonstrate the feasibility of HSI for precise varietal mapping, which can support more efficient and sustainable orchard management practices.

In Section 2, we present related work and describe the methods employed, including a brief review of similar studies and the workflow followed for data processing. Section 3 discusses the results obtained after applying the proposed classification methods for olive variety differentiation. Section 4 provides an evaluation and discussion of the results, while Section 5 concludes the study and outlines potential directions for future research.

II. Related work | Methods

HSI has become a key technology in precision agriculture, providing a non-destructive and high-resolution method for crop monitoring and analysis [1]. Unlike multispectral imaging, it captures reflectance across numerous narrow spectral bands, detecting subtle differences often missed by traditional sensors [2]. Applications include soil erosion analysis, plant health assessment, and water stress monitoring [3], as well as inventory management, irrigation control, disease detection, and yield estimation in olive cultivation [4], contributing to sustainable practices by optimizing resources and reducing environmental impact [5].

HSI's detailed chemical and physical information makes it particularly effective for distinguishing crop varieties [6]. It has been used to identify crop types like wheat, maize, and rice [7] [8], and even different varieties within the same crop, such as wheat [9] and rice [10]. In olive cultivation, beyond variety identification, HSI has supported disease detection, maturity assessment, and yield estimation [11] [12].

Given the diversity of olive varieties, HSI-based classification is a growing research field. By capturing differences in pigment concentration, moisture, and cellular structure, hyperspectral sensors can distinguish varieties, although challenges remain due to spectral similarities and external factors. Recent studies have shown the feasibility of variety identification using lightweight models throughout the season [13] [14].

Gomes et al. [15] demonstrated that hyperspectral reflectance effectively differentiates olive varieties, emphasizing its value for sustainable orchard management. Unlike manual spectral acquisition, our approach uses UAV-mounted sensors for automated, large-scale mapping without laboratory sampling.

However, UAV-based HSI faces challenges such as the influence of shadows on vegetation indices [16] and the need for improved hyperspectral mosaicking methods [17]. Addressing these issues is crucial to fully exploit HSI for olive variety identification and precision agriculture.

Figure 1 shows the general workflow followed by the methodology.

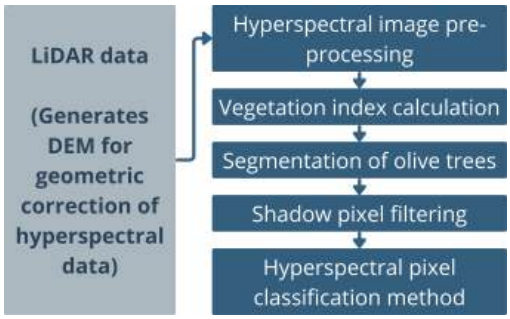

Figure 1. Methodology workflow.

The study was conducted in Mengíbar, Jaén, at the IFAPA Venta del Llano Center, a research facility focused on agricultural development, particularly olive cultivation. Its location is shown in Figure 2. The experimental plot consists of 14 rows of olive trees, each with approximately 24 trees, organized into blocks of four trees per variety. Among these, 21 different olive varieties are tested, including 'Arbequina' and 'Picual' as reference cultivars. The randomized distribution ensures representative data collection, aiding research on adaptability, productivity, and phenotypic characteristics.

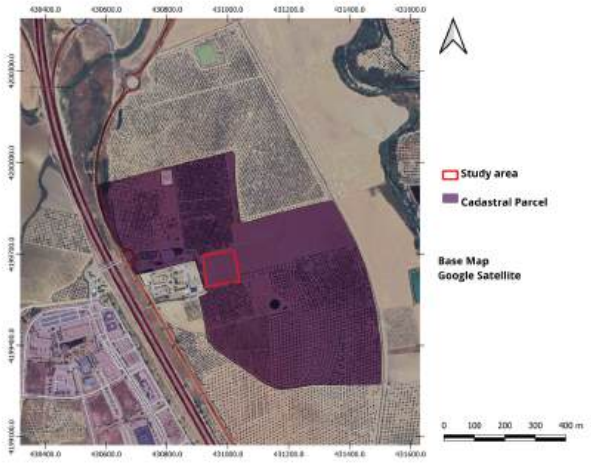

Figure 2. Geogrphic location for the study area.

A UAV equipped with a NanoHyperspec camera (Headwall) and a Light Detection And Ranging (LiDAR) sensor captured hyperspectral data across 270 spectral bands (400–1000 nm) at a 2 cm Ground Sample Distance (GSD). The flight was conducted at 30 meters AGL with a speed of 5 m/s, ensuring high data quality. Overlapping flight paths (1% longitudinal, 40% lateral) minimized gaps, while terrain adjustments maintained accuracy. Headwall SpectralView™ software processed the hyperspectral data, applying radiometric and geometric corrections using a Digital Elevation Model (DEM) derived from LiDAR data. The reflectance calibration was based on dark and white reference measurements. Figure 3 shows the processes required to properly correct the data taken with the hyperspectral sensor.

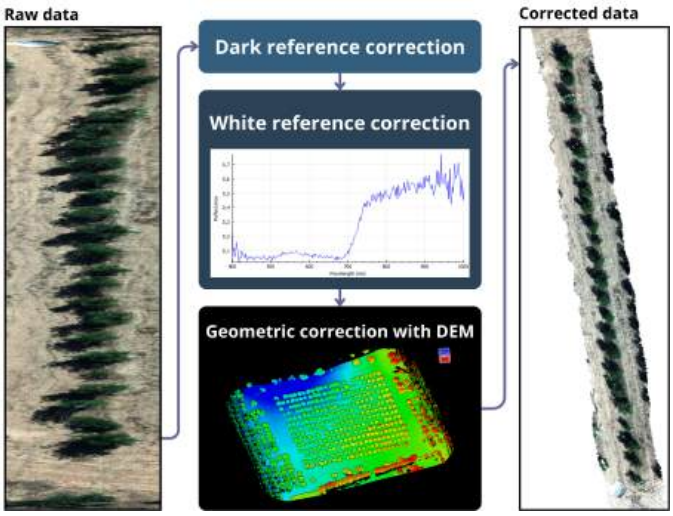

Figure 3. Spectral and geometric corrections applied to the hiperspectral data.

Once the hyperspectral data is properly adjusted, it is necessary to differenciate invidual olive trees, applying a tree canopy segmentation. Individual tree segmentation was essential for precise spectral analysis. Using the Enhanced Vegetation Index (EVI), vegetation was isolated, minimizing shadow effects. EVI was selected due to its effectiveness in distinguishing vegetation while minimizing shadow influence. The index's smoothing term (L) reduces soil background effects, which is particularly useful in olive orchards. By utilizing specific spectral bands (*Near-Infrared* (NIR), red, and blue), EVI is particularly well-suited for analyzing hyperspectral image data, where these bands are clearly defined [18].

The equation is as follows:

$$\text{EVI} = G \cdot \frac{\text{NIR} - \text{Red}}{\text{NIR} + C_1 \cdot \text{Red} - C_2 \cdot \text{Blue} + L}, \qquad (1)$$

where:

- G: Gain factor, with a default value of 2.5
- C_1 y C_2: Atmospheric correction coefficients, with default values of 6.0 and 7.5, respectively.
- L: Smoothing term, with a default value of 1.0.

Once the pixels of interest are selected, the segmentation is refined by delineating olive trees more precisely using several geospatial processing techniques and clustering methods. The key method for this segmentation is the use of the *Density-Based Spatial Clustering of Applications with Noise* (DBSCAN) algorithm for grouping geometries into individual trees [19]. This process generates a vector mask with unique identifiers

and variety classifications. The final segmentation was manually refined in the software *Quantum Geographic Information System* (QGIS) to ensure accuracy [20]. Figure 4 shows the steps taken to properly segment trees canopies.

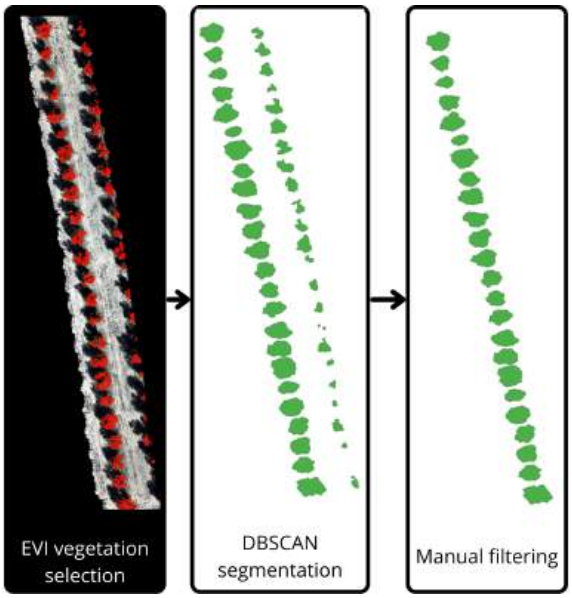

Figure 4. Segmentation process.

Once the olive canopy is identified, selecting relevant hyperspectral pixels is critical for improving classification accuracy. A two-step filtering process is applied: first, low-reflectance pixels, mainly from shadowed areas, are removed based on NIR reflectance thresholds; second, spectral stability is ensured by filtering out pixels with high variability across bands.

In the first step, pixels are assessed by their NIR reflectance, retaining only those exceeding a predefined threshold to exclude shadow-affected areas. The second step refines pixel selection by evaluating spectral variability. Two statistical parameters are computed for each band:

- **Spectral Relevance Threshold**: pixels are considered relevant if its reflectance value exceeds a dynamically calculated threshold:

$$\text{threshold}_{\text{mean}}[band] = \mu[band] + 0.5 \cdot \sigma[band]$$

- **Low Dispersion Criterion**: to ensure that selected pixels belong to bands with limited variability, an additional constraint is applied:

$$\sigma[band] < 0.75 \cdot \overline{\sigma}$$

where $\overline{\sigma}$ represents the global mean standard deviation across all bands. This condition excludes spectral bands with excessive variability, which may be less reliable for analysis.

Pixels meeting both criteria are retained, resulting in a binary mask that refines the dataset by eliminating spectral inconsistencies. As shown in Figure 5, these filters are applied to each tree to exclude pixels affected by shadows or extreme spectral responses, ensuring a more accurate and representative analysis.

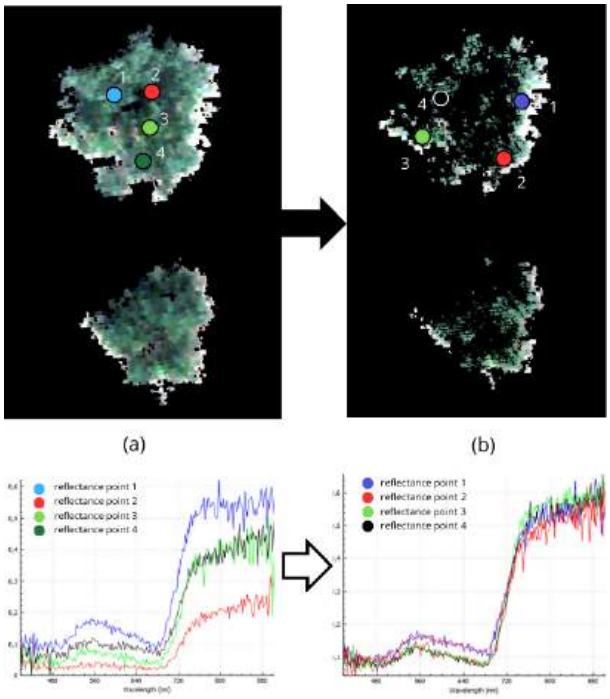

Figure 5. Before and after applying low reflectance filtering in the NIR and standard deviation. (a) Unfiltered view of Olive 401 and the reflectance response of randomly selected pixels. (b) View of Olive 401 after filtering and the reflectance response of randomly selected pixels.

To compare different olive trees and determine whether they exhibit similar spectral behaviour, a classification system based on spectral ranges was developed. This method operates at both the pixel and tree levels, calculating the percentage of pixels within each predefined range for each tree. To optimize computational efficiency, spectral bands were selectively sampled: one out of every ten bands, and one out of every five in the NIR region, where vegetation reflectance is most sensitive to variations. This resulted in a total selection of 27 bands.

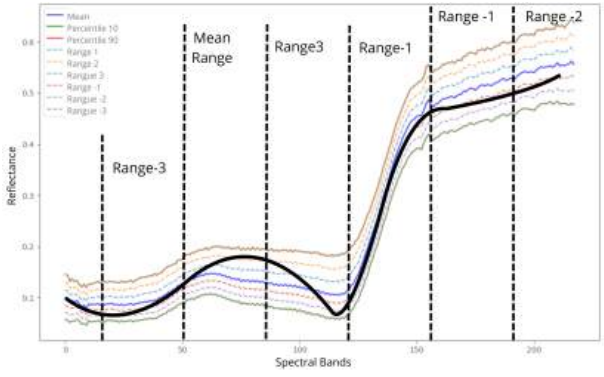

Figure 6. Comparison of any spectral response with the created ranges. Each spectral signature falls within a different range for each of the selected spectral bands.

The classification approach is based on a reference spectral signature constructed from the mean spectral response of all analysed olive trees. From this baseline, upper and lower thresholds are defined using the 90th and 10th percentiles, respectively. This ensures the exclusion of extreme pixel values that might distort classification results. Each pixel's spectral signature is compared against the baseline across the selected bands, classifying it into six ranges. Figure 6 illustrates a sample spectral reflectance response compared to the predefined ranges, indicating the corresponding range for each selected band. This information is then used to classify all pixels within the canopy of each tree.

TABLE I
VALUES BY ID_OLIVE AND THEIR RESPECTIVE RANGES.

ID_OLIVE	Variety	Range	10	20	30	...	217
401	36-41	Max range (Range 3 to 10.0)	19.86	18.29	18.92	...	3.10
401	36-41	Range 3 / Range 2	9.60	7.93	9.56	...	4.44
401	36-41	Range 2 / Range 1	13.31	10.50	10.14	...	8.91
401	36-41	Range 1 / Mean	16.25	16.19	15.32	...	14.06
401	36-41	Mean / Range -1	15.07	16.11	15.14	...	16.82
401	36-41	Range -1 / Range -2	12.12	13.34	14.71	...	17.41
401	36-41	Range -2 / Range -3	7.65	10.36	10.17	...	15.01
401	36-41	Min range (0.0 to Range -3)	6.13	7.29	6.04	...	20.27

The classification results are organized in a matrix where the x-axis represents the 27 spectral bands and the y-axis the defined ranges. Each cell shows the percentage of pixels falling within each range for a given band. For example, if all pixels of a band fall into range 2, it will account for 100% of the pixels, with the rest at 0%.

This classification enables the analysis of the pixel distribution across ranges for each tree, allowing comparative assessments of spectral behaviour between different olive trees and varieties. Results are systematically stored and analysed, providing a quantitative basis for evaluating varietal differences. As shown in Table I, the percentage distribution across ranges is displayed for each selected band, ensuring that the total per band sums to 100.

III. RESULTS

Following the implementation of the classification method for the hyperspectral image, numerical results were obtained, providing insights into the distribution of pixels within each olive tree across different predefined spectral ranges. By analyzing these proportions, comparisons were made between olive trees of similar and different varieties to identify potential differences in their spectral behaviour.

Given the complexity of interpreting numerical differences directly, graphical representations were employed. As shown in Figure 7, pixel proportions per spectral band were visualized for each created range, using olive tree 401 as an example. The graph is divided into six sections, each corresponding to a different range, illustrating the distribution of pixel proportions across spectral bands. A clear trend is observed, where most pixels are concentrated in intermediate ranges.

This graphical representation was extended to all 24 olive trees in the study row, with every four trees belonging to the same variety. The objective was to determine whether trees of the same variety exhibited similar trends in their spectral distributions. Figure 8 displays all graphical representations, where each set of four graphs corresponds to a specific variety.

Upon analysing the spectral distributions of the 24 olive trees, clear patterns emerged within each variety. Notably, Arbequina and Picual varieties exhibited consistent spectral trends, with similar curve shapes and peak amplitudes among trees of the same variety. These findings suggest that spectral characteristics, influenced by the biophysical and biochemical properties of the trees, are closely related to variety, reinforcing the idea that genetic and physiological factors impact spectral behaviour.

According to IFAPA farm organizers, the studied varieties originate from the same maternal lineage, implying genetic similarity. However, differences were observed between two groups of Picual trees, indicating variability despite belonging to the same variety. This discrepancy may be attributed to the fact that these groups do not share the same mother plant, potentially resulting in distinct genomes that explain the spectral differences. Consequently, trees within each subgroup

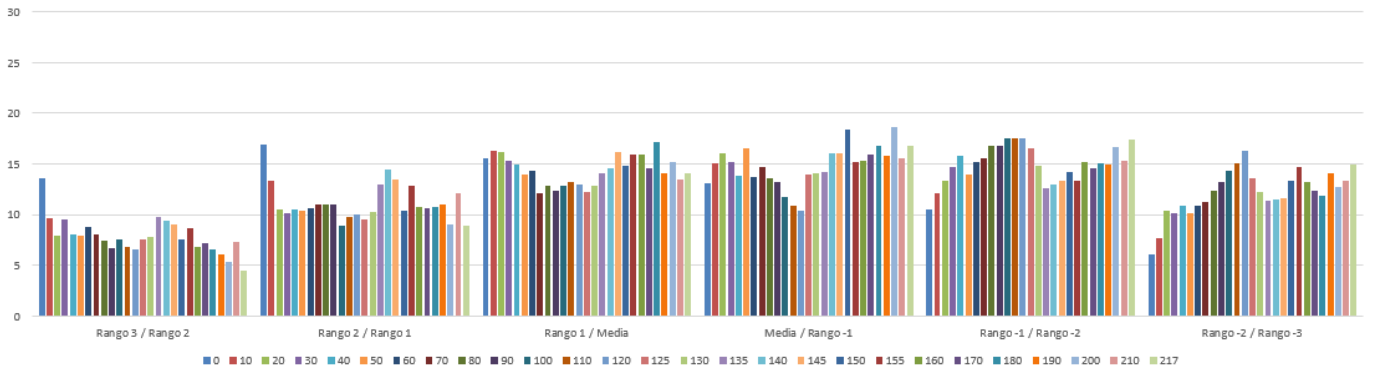

Figure 7. Graphical representation of the proportion of pixels in each range for a random olive tree.

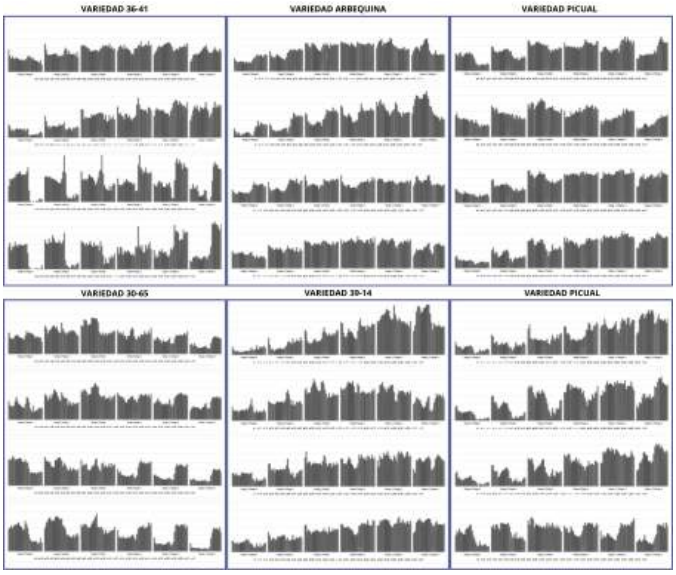

Figure 8. Representation of proportion graphs for each olive tree (24 in total).

are expected to be more similar to each other than to those in the other subgroup.

Additionally, minor variations were noted within each variety, likely influenced by external factors such as lighting conditions or localized environmental differences. These variations were more pronounced in the 36-41 variety, where certain spectral peaks displayed greater fluctuation. Despite these variations, the overall pattern remained consistent, reinforcing the potential of HSI as a reliable tool for olive variety differentiation, as is shown in Figure 8.

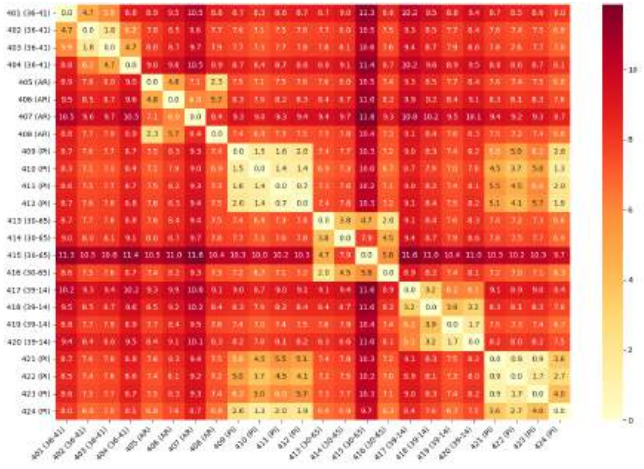

Figure 9. Heatmap of Euclidean distances between olive trees based on extracted features (mean, standard deviation, maximum, minimum, skewness, and kurtosis). Lighter colors (yellow) indicate smaller distances (higher similarity), and darker colors (red) indicate larger distances (lower similarity). Olive trees are labeled with their ID and variety (e.g., "401 (36-41)").

To further explore the similarities and differences among olive trees, a heatmap of pairwise Euclidean distances in a normalized feature space was generated, as is shown in Figure 9. Features including the mean, standard deviation, maximum, minimum, skewness, and kurtosis were extracted from the spectral data for each olive tree and standardized. The olive trees are compared to each other, generating this heat map, which visualizes these distances, with lighter colors (yellow) indicating higher similarity and darker colors (red) indicating greater dissimilarity. For instance, olive trees of the same variety, such as 403 and 404 (both "36-41"), show small distances, while trees from different varieties, such as 403 ("36-41") and 405 ("AR"), exhibit larger distances. A Random Forest classifier validated these features, achieving an accuracy of 1.0 across 5-fold cross-validation, confirming their effectiveness in distinguishing olive varieties. It is visible as well how the first four olives with variety PI (Picual) shown similarities with the last four olives of the same variety.

This analysis highlights the significance of Hyper-Spectral Imaging in varietal classification, as intra-varietal similarities were found to be substantial despite minor fluctuations. These findings support the use of spectral analysis for the classification and management of olive varieties in agricultural settings.

IV. Discussion | Evaluation

This study demonstrates the effectiveness of UAV-based Hyper-Spectral Imaging (HSI) for differentiating olive varieties based on spectral characteristics. The successful classification of Arbequina and Picual varieties highlights the potential of spectral analysis as a non-invasive tool for varietal identification.

Critical to this success were spectral filtering and advanced segmentation techniques, which minimized noise by removing shadow-affected pixels and applying spectral stability criteria. However, environmental factors such as illumination variability, atmospheric conditions, and leaf age remain challenges that can introduce inconsistencies.

Overall, the evaluation of the results obtained is positive. Not only was the spectral similarity between olive trees of the same variety intuited in the graphs shown in Figure 8, but the comparison of olive trees using the Euclidean distance calculation clearly shows the similarity between these varieties, clearly visualized in the matrix in Figure 9, taking into account the specific failures that are difficult to distinguish due to the environmental factors described above.

It can therefore be confirmed that UAV-based HSI offers valuable advantages for precision agriculture by enabling large-scale varietal monitoring, supporting more efficient orchard management, and promoting sustainable olive production.

V. Conclusion and Future Work

This work establishes UAV-based hyperspectral imaging as a scalable and effective method for olive variety classification, offering a promising alternative to traditional sampling approaches. Despite its success, environmental variability and computational demands must be addressed to fully unlock its potential.

Future research should focus on enhancing model robustness against external factors through advanced machine learning

techniques, particularly deep learning models capable of capturing subtle spectral patterns. Improving computational efficiency using dimensionality reduction methods, such as autoencoders or a *Principal Component Analysis* (PCA), will be key to enabling real-time or near-real-time analysis.

Additionally, the fusion of hyperspectral data with other sensing modalities, like LiDAR or thermal imaging, presents a promising path for improving the differentiation of similar cultivars. Advances in these areas will drive the broader adoption of HSI in agriculture, fostering more precise, efficient, and sustainable orchard management.

ACKNOWLEDGMENTS

This research has been partially funded through the research support provided by the Ministry of Innovation and Science of the Government of Spain through the research project PID2021-126339OB-I00 and from the European Union's Horizon Europe research and innovation programme under the grant agreements No. 101157502 (Soil Deal for Europe - HORIZON-MISS-2023-SOIL-01).

REFERENCES

[1] L. Shuai, Z. Li, Z. Chen, D. Luo, and J. Mu, "A research review on deep learning combined with hyperspectral imaging in multiscale agricultural sensing", *Computers and Electronics in Agriculture*, vol. 217, p. 108 577, Feb. 1, 2024, ISSN: 0168-1699. DOI: 10.1016/j.compag.2023.108577.

[2] K. E. Karfi, S. E. Fkihi, L. E. Mansouri, and O. Naggar, "Classification of hyperspectral remote sensing images for crop type identification: State of the art", *Proceedings of the 2nd International Conference on Advanced Technologies for Humanity*, 2020. DOI: 10.5220/0010426600110018.

[3] G. Messina and G. Modica, "Twenty years of remote sensing applications targeting landscape analysis and environmental issues in olive growing: A review", *Remote. Sens.*, vol. 14, p. 5430, 2022. DOI: 10.3390/rs14215430.

[4] P. Marques, L. Pádua, J. J. Sousa, and A. A. Fernandes-Silva, "Advancements in remote sensing imagery applications for precision management in olive growing: A systematic review", *Remote. Sens.*, vol. 16, p. 1324, 2024. DOI: 10.3390/rs16081324.

[5] M. Govender, K. Chetty, V. Naiken, and H. Bulcock, "A comparison of satellite hyperspectral and multispectral remote sensing imagery for improved classification and mapping of vegetation", *Water sa*, vol. 34, no. 2, pp. 147–154, 2008. DOI: 10.4314/wsa.v34i2.183634.

[6] M. R. R. d. Oliveira, S. G. Ribeiro, J.-F. Mas, and A. d. S. Teixeira, "Advances in hyperspectral sensing in agriculture: A review", *revista ciencia agronomica*, 2020. DOI: 10.5935/1806-6690.20200096.

[7] R. N. Sahoo, S. Ray, and K. Manjunath, "Hyperspectral remote sensing of agriculture", *Current science*, pp. 848–859, 2015.

[8] F. Zhang *et al.*, "Hyperspectral imaging combined with CNN for maize variety identification", *Frontiers in Plant Science*, vol. 14, p. 1 254 548, 2023. DOI: 10.3389/fpls.2023.1254548.

[9] A.-K. Mahlein *et al.*, "Development of spectral indices for detecting and identifying plant diseases", *Remote Sensing of Environment*, vol. 128, pp. 21–30, 2013. DOI: 10.1016/j.rse.2012.09.019.

[10] B. Jin *et al.*, "Identification of rice seed varieties based on near-infrared hyperspectral imaging technology combined with deep learning", *ACS omega*, vol. 7, no. 6, pp. 4735–4749, 2022. DOI: 10.1021/acsomega.1c04102.

[11] T. Poblete *et al.*, "Discriminating xylella fastidiosa from verticillium dahliae infections in olive trees using thermal-and hyperspectral-based plant traits", *ISPRS Journal of Photogrammetry and Remote Sensing*, vol. 179, pp. 133–144, 2021. DOI: 10.1016/j.isprsjprs.2021.07.014.

[12] C. Riefolo *et al.*, "Assessment of the hyperspectral data analysis as a tool to diagnose xylella fastidiosa in the asymptomatic leaves of olive plants", *Plants*, vol. 10, no. 4, p. 683, 2021. DOI: 10.3390/plants10040683.

[13] G. Moreda, J. Ortiz-Cañavate, F. J. García-Ramos, and M. Ruiz-Altisent, "Non-destructive technologies for fruit and vegetable size determination–a review", *Journal of Food Engineering*, vol. 92, no. 2, pp. 119–136, 2009. DOI: 10.1016/j.jfoodeng.2008.11.004.

[14] S. Domínguez-Cid *et al.*, "Identification of olives using in-field hyperspectral imaging with lightweight models", *Sensors (Basel, Switzerland)*, vol. 24, 2024. DOI: 10.3390/s24051370.

[15] L. Gomes, T. Nobre, A. M. O. Sousa, F. T. Rei, and N. Guiomar, "Hyperspectral reflectance as a basis to discriminate olive varieties—a tool for sustainable crop management", *Sustainability*, 2020. DOI: 10.3390/su12073059.

[16] L. Zhang, X. Sun, T. Wu, and H. Zhang, "An analysis of shadow effects on spectral vegetation indexes using a ground-based imaging spectrometer", *IEEE Geoscience and Remote Sensing Letters*, vol. 12, no. 11, pp. 2188–2192, Nov. 2015, ISSN: 1558-0571. DOI: 10.1109/LGRS.2015.2450218.

[17] J. M. Jurado, L. Pádua, J. Hruška, F. R. Feito, and J. J. Sousa, "An efficient method for generating UAV-based hyperspectral mosaics using push-broom sensors", *IEEE Journal of Selected Topics in Applied Earth Observations and Remote Sensing*, vol. 14, pp. 6515–6531, 2021, ISSN: 2151-1535. DOI: 10.1109/JSTARS.2021.3088945.

[18] B. D. Wardlow, S. L. Egbert, and J. H. Kastens, "Analysis of time-series MODIS 250 m vegetation index data for crop classification in the US central great plains", *Remote sensing of environment*, vol. 108, no. 3, pp. 290–310, 2007, Publisher: Elsevier.

[19] M. Ester, H. P. Kriegel, J. Sander, and X. Xiaowei, "A density-based algorithm for discovering clusters in large spatial databases with noise", in *Proceedins of the international conference on knowledge discovery and data mining*, AAAI Press, Menlo Park, CA (United States), Dec. 1996.

[20] QGIS Development Team, *QGIS Geographic Information System*. Open Source Geospatial Foundation, 2009.